ACS OMEGA

Article

Cite This: ACS Omega 2018, 3, 12482−12488

http://pubs.acs.org/journal/acsodf

Quantitative Tracking of the Oxidation of Black Phosphorus in the Few-Layer Regime

Juan Gómez-Pérez,[†] Balázs Barna,[†] Ildikó Y. Tóth,[†,‡] Zoltán Kónya,[†,§] and Ákos Kukovecz*[,†,‡]

[†]Department of Applied and Environmental Chemistry, University of Szeged, Rerrich Béla tér 1, H-6720 Szeged, Hungary

[‡]SZTE "Lendület" Porous Nanocomposites Research Group, Rerrich Béla tér 1, H-6720 Szeged, Hungary

[§]MTA-SZTE Reaction Kinetics and Surface Chemistry Research Group, Rerrich Béla tér 1, H-6720 Szeged, Hungary

Supporting Information

ABSTRACT: Previous theoretical reports have described the oxidation of few-layer black phosphorus and its effects on the electronic properties. Theoretically, native oxide layers bring opportunities for band gap engineering, but the detection of the different types of oxides is still a challenge at the experimental level. In this work, we uncover a correlation between thermal processes and Raman shift for the A_g^1, B_{2g}, and A_g^2 vibrational modes. The thermal expansion coefficients (temperature range, 290−485 K) for the A_g^1, B_{2g}, and A_g^2 were −0.015, −0.027, and −0.028 cm^{-1} K^{-1}, respectively. Differential scanning calorimetry analysis shows an endothermic process centered at 528 K, and it was related with a mass increase according to thermogravimetric analysis. Raman shift temperature dependence was correlated to theoretical lattice thermal expansion, and a significant deviation was detected in the stacking direction at 500 K.

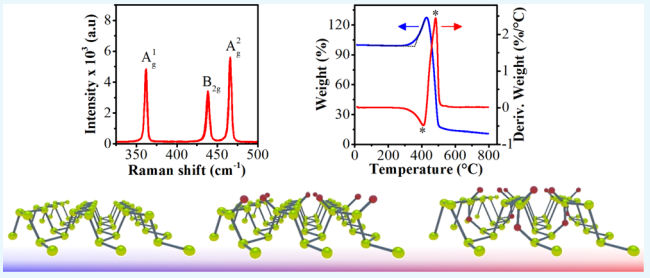

1. INTRODUCTION

Exfoliated black phosphorus (BP) is an anisotropic p-type semiconductor[1,2] with interesting properties: hole mobility between 100 and 1000 cm^2 V^{-1} s^{-1},[3] on/off ratio at room temperature between 10^2 and 10^5,[2] and tunable direct band gap between 0.3 eV in the bulk phase and 2.2 eV for the monolayer.[4,5] The band gap modulation of black phosphorus ranges between the defect-induced band gaps of graphene (0 to ∼0.3 eV[3]) and the typical values for transition-metal dichalcogenides;[3,6,7] therefore, during the past years, BP has been recognized as a promising material for electronic and optoelectronic devices.[8]

Black phosphorus offers several opportunities for applications: water splitting,[9] nanoresonators,[10] and gas sensing[11] are some examples. Nevertheless, prompt oxidation, in comparison to other 2D materials,[12−17] is among its biggest challenges. Oxidation in BP may cause dramatic structural transformations,[5,18−20] but controlled oxidation can be useful to engineer its electronic properties,[7,13,21] increase its environmental stability by passivation,[5,20,22,23] or ease its reaction with certain molecules.[18,24]

The chemisorption of oxygen dimers (O_2) over BP can be affected by visible light, as the potential barriers decrease from larger than 10 eV in pristine surfaces to less than 6 eV at intrinsic defect sites.[25,26] Experimentally, the effect of light on oxidation has been proven, and samples stored in the dark show lower rates of degradation.[27] Edmonds et al., working on air-oxidized bulk BP crystal, demonstrated the presence of several types of oxides[20] in agreement with theoretical studies.[5] Nevertheless, phosphorus pentoxide (i.e., $O'-(P_2O_5)_\infty$) is considered to be the most stable form of oxide.[5,28]

Light, water, and oxygen are the environmental factors required for oxidation of black phosphorus according to theoretical[18,25] and experimental[23,27,29,30] studies. Favron et al. proved that independently, neither visible light in a vacuum (5×10^{-6} torr) nor oxygen and water can induce any degradation on black phosphorus detectable by conventional Raman spectroscopy (2×10^4 W cm^{-2} at λ = 532 nm).[27] Similarly, Woomer et al. confirmed the role of light (λ = 460 nm) in the oxidation process by using X-ray photoelectron spectroscopy (XPS) measurements and oxygen (not dried) exposure. The oxidation was evident from the broadening of the peak at 133 eV.[29]

The oxidation of black phosphorus modifies the electronic properties of the material, but the degree of modification depends on the type of the formed oxide. Different kinds of modifications are expected: lattice parameter variations;[5,25,28,31] vibrational energy variations due to the presence of oxygen bound in dangling or bridging configurations;[18] and electronic property variations,[20] depending on the type of oxide, degree of oxidation,[2] and local geometry.[25]

Theoretical studies[5,18,22,32] predicted the formation of oxygen bonding in dangling, bridging, and interstitial configurations (Figure 1). Dangling and interstitial oxygen bonds are electrically neutral, but the bridging configurations

Received: August 10, 2018
Accepted: September 20, 2018
Published: October 3, 2018

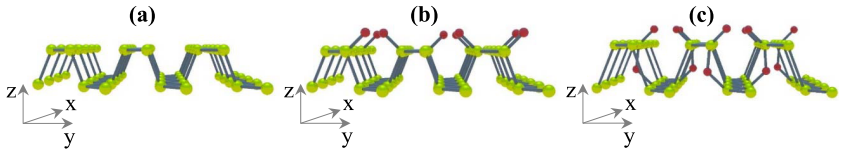

Figure 1. Oxidized black phosphorus forms. Pristine monolayer (a), surface dangling oxygen (red)—BP oxide (b), and interstitial and dangling oxygen configurations (c).

create levels in the gap.[18,21] Interstitial oxygen is characterized by higher lattice distortions,[18] and dangling oxygen configuration is energetically favored for lower oxygen concentrations.[5,18] However, the Coulomb repulsion between oxygen p orbitals is higher for the dangling type of oxides;[5] therefore, the orientation of the P═O bonds always points away in different directions from the zigzag ridge, in which they are chemisorbed.[5,18,25]

The band gap engineering of phosphorene has been proposed by different methods: modification of the external conditions (i.e., electric bias, mechanical strain),[9] functionalization,[32] heterostructures,[2] passivation,[16,20,27,32,33] oxidation,[5,7,21,22,34] and changes in local geometry[7,25] are some examples. For instance, BP-controlled oxidation or passivation with h-BN can induce higher hole or electron mobilities, respectively,[2] and oxidation or doping with H_2 and F_2 changes the band gap from direct to indirect.[5,21,32] In general, some similarities have been pointed out for highly oxidized forms (*t*-P_4O_{10} and *p*-P_4O_{10}): the valence and conduction bands always come from the oxygen p orbitals (e.g., in dangling and bridging configurations),[5] the higher occupied levels are degenerate dispersionless states, and the conduction bands are slightly dispersive.[5] These features are of importance as the tuning of the band gap increases the stability of the material[25] and the feasibility for applications.[9,23] Theoretically, differences have been pointed out in comparison between interstitial (planar) and surface oxides: the average binding energy (E_b) of the material depends on the number of oxygens in the unit cell, but the E_b of the surface oxide is lower than that of the interstitial (planar) counterpart by approximately 0.7 eV.[5]

In phosphorene band gap engineering, "*the issue seems to be how oxidation is detected*", as stated by Ziletti et al.[18] Conventional Raman spectroscopy has been useful for different purposes in the research of black phosphorus: exfoliation,[4,16,35,36] alkali intercalation,[37] annealing,[38] photo-oxidation,[27] and functionalization/passivation[39,40] are some examples. However, the theoretically predicted variety of oxidized species has not been detected by Raman spectroscopy yet. The present work demonstrates a correlation between theoretical studies, thermal analysis, and conventional backscattering Raman spectroscopy and contributes to the understanding of the oxidation process in black phosphorus.

2. RESULTS AND DISCUSSION

The suspensions produced through liquid-phase exfoliation (LPE) were characterized by DLS, and the results are shown in Table 1. All of the samples were stable with apparent zeta potentials larger than 30 mV. The average hydrodynamic size was controlled by increasing centrifugation speeds, as described in the Methods section. Previous results demonstrate that acetone can be used for the exfoliation of black phosphorus with good reproducibility of the basic features (size, thickness, and stability). The produced material is easier to handle and clean than that obtained with other solvents

Table 1. Characterization for the Exfoliated and Centrifuged Material

sample	hydrodynamic size (nm)[a]	zeta potential (mV)[a]	optical band gap (eV)[b]
AsEx	230	−42.3 ± 0.27	1.48
BP2S	146	−35.8 ± 0.92	1.95
BP4S	96	−38.1 ± 0.32	2.15

[a]Measured with dynamic light scattering. [b]Estimated from the UV−vis−NIR spectra.

such as NMP or CHP. In our previous work,[41] we have shown the topographical characteristics of the flakes produced with LPE in acetone. The correlation between atomic force microscopy (AFM) measurements and hydrodynamic sizes constitute an operational advantage at the moment of characterizing the material because DLS is considerably faster than atomic force microscopy.

The optical band gaps of the exfoliated materials are shown in Table 1. The close match between the optical band gap of the sample BP4S and the theoretical electronic band gap of the monolayer (E_g: 2.2 eV[4,42]) is explained by the relationship between the exciton binding energy and the dielectric constant of the medium.[29] For exfoliated black phosphorus in acetone (dielectric constant, ε = 20.7), the exciton binding energy is expected to be −31.1 meV.[29] From these results, we conclude that our suspensions are mixtures of monolayers, bilayers, and trilayers and that their composition varies toward the isolated monolayers with increasing rotational frequency during centrifugation.[41] This is an important characteristic of the sample as the collected Raman spectra have less or no interference from inner flakes in the crystalline structure.

2.1. Thermal Analysis of Bulk Black Phosphorus Oxidation. Thermogravimetric curves for bulk BP in oxidative media (synthetic air) are presented in Figure 2. The onset temperature of the mass increase was 630 K (Figure 2a). Additionally, two samples were tested at different heating ramps: 5 K min^{-1} (Figure 2a,b) and 10 K min^{-1} (not shown). The weight derivatives show a starting point for the mass increase at approximately 493 K (Figure 2b). The sample decomposition, measured as a mass decrease, was predominant at approximately 703 K (Figure 2a). The first derivative peaks were located at approximately 683 and 753 K, and they indicate the temperatures of the greatest rate of mass increase and decrease, respectively (Figure 2a). These results are in agreement with those obtained by Liu et al., using in situ scanning/transmission electron microscopy, as the selective area electron diffraction patterns for exfoliated black phosphorus, but with thicknesses between 10 and 40 nm, show decomposition, which starts at approximately 673 K.[43]

Differential scanning calorimetry (DSC) measurements were done with aluminum sample holders (pan + lid) in a controlled nitrogen atmosphere. Two different processes were detected during the heating cycle (Figure 2c): one endothermic process centered at approximately 528 K and one exothermic peak

DOI: 10.1021/acsomega.8b01989
ACS Omega 2018, 3, 12482−12488

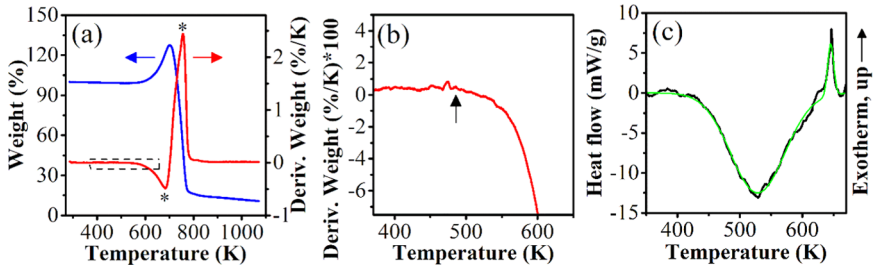

Figure 2. Thermogravimetric analysis (TGA) for bulk BP in oxidative media (synthetic air). Onset temperatures are calculated from the linear extrapolation before and after the inflection point (a). Details of the dashed region in (a) (heating ramp: 5 K min^{-1}) (b). The arrow in (b) indicates a temperature of 493 K. Differential scanning calorimetry from the bulk starting material (black) and the peak fitting output (green) (nitrogen media, heating ramp: 5 K min^{-1}; aluminum pan and lid) (c).

centered at approximately 643 K. The measured endothermic process was broad (full width at half-maximum (FWHM): 101 K) and started at approximately 423 K. The exothermic peak was 10 times sharper (FWHM: 100 K), had low intensity (approximately 5.2 mW g^{-1}), and was detectable at almost the same temperature with the maximum rate of oxygen uptake, as seen from the TGA measurements in oxidative media (Figure 2a,b). In the literature, two processes were found to be exothermic: (1) the oxygen chemisorption on black phosphorus[18,24,25,32,34] and (2) the formation of interstitial oxygen bridges.[18] We suppose that the exothermic peak relates with oxygen chemisorption as it was available for the sample before it was closed in the holder of the DSC measurement. The cooling cycle was exothermic (not shown) and can be interpreted as reversibility of the broad endothermic peak shown in Figure 2c.

The nature of the endothermic process is uncertain, but the melting-crystallization process is unlikely since the melting temperatures of black and red phosphorus are 873 and 893 K, respectively.[44] Liu et al. reported a thermal-induced increase of the lattice parameters of exfoliated black phosphorus[43] in the same temperature range as our DSC measurements. On the other hand, Ziletti et al., based on theoretical calculations, reported that the binding energies of interstitial and dangling oxides are −1.66 and −2.08 eV at PBE level, respectively,[18] and transformation from dangling to interstitial oxygen requires 0.69 eV via oxygen penetration into the lattice.

On the basis of these evidences, we suggest that the endothermic process is caused by the lattice thermal expansion[43] and subsequent formation of interstitial oxygen bonding as larger and weaker P−P bonds favor interstitial oxygen formation. In a second step, the new configuration reduces the Coulomb repulsion[5] and allows higher oxygen incorporation as seen in the TGA (Figure 2), giving place to the calculated planar type of oxides (Figure 1c). Summarizing, we propose that the transitions visible in the thermal analysis evidence transformations from surface to interstitial type of oxides, possibly at intrinsic defects since the thermal energy involved is not enough to induce the transition in defect-free surfaces. The consequences of this suggestion are confirmation of the higher stability of surface (dangling or bridging) over the interstitial type of oxides and supporting the understanding of the following results with Raman spectroscopy.

2.2. Few-Layer Black Phosphorus Oxidation. The typical Raman spectrum for the bulk starting material is shown in Figure 3a. The following results were obtained from measurements with a backscattering configuration. According to calculated phonon dispersion curves, the A_g^1, B_{2g}, and A_g^2 vibrational modes are visible in the first Brillouin zone and oscillate along the *z*, *y*, and *x* directions, respectively.[7,17] Ziletti et al., in theoretical studies,[5,18] described vibrational modes at 1099 cm^{-1} for dangling oxygen, 574 and 763 cm^{-1} for interstitial oxygen, and no vibrational modes between 500 and 1000 cm^{-1} for surface oxides. However, for surface oxides, they predicted a blue shift in the P═O stretching mode region (1063 cm^{-1}) with increasing oxygen concentration until reaching approximately 1370 cm^{-1},[5] but these modes have not been detected with conventional Raman spectroscopy.

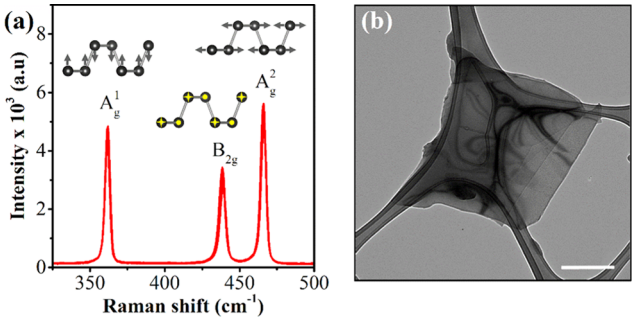

Figure 3. Raman characterization for the bulk starting material and the representation of the visible vibrational modes (a). Transmission electron microscopy (TEM) image of the few-layer black phosphorus (AsEx) (b). The scale bar is 500 nm.

Raman spectroscopy has been used to evaluate exfoliation processes by measuring blue shift in the position of the vibrational modes, but its applicability in that purpose is still not fully accepted.[7,27] Lower intensities in the Raman shift spectra, lower A_g^1/A_g^2 intensity ratios, and the emergence of broad features between the B_{2g} and A_g^2 vibrational modes have been identified as signatures of oxidation.[16,17,27] On the other hand, the blue shift in the Raman spectra of black phosphorus has been related with thermal annealing processes of exfoliated materials (thickness: approximately 15 nm)[38] and degradation of thick samples (thickness >35 nm).[45]

The TEM image presented in Figure 3b shows a good agreement with the DLS (Table 1) and previous AFM measurements.[41] The study of disordered graphene has been recognized as a strong necessity for practical progress.[46] In this work, we evaluate the oxidation of polycrystalline samples of few-layer phosphorene. This sample preparation allows larger-area coverage for easier scalability.

Previously, the correlation between oxygen content and electronic properties has been discussed.[5,13] In addition to the prediction of electrically neutral oxides,[18] Malyi et al. stated that oxygen-poor compounds can be considered as "black

DOI: 10.1021/acsomega.8b01989
ACS Omega 2018, 3, 12482−12488

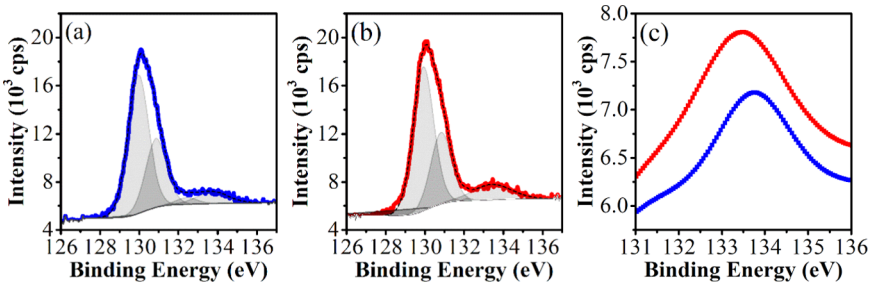

Figure 4. XPS measurements for acetone-exfoliated black phosphorus (AsEx). Starting point (a) and 21 days later (b). Details for the deconvolution region at 133.5 eV for the sample at the starting point (blue) and 21 days later in air (red) (c).

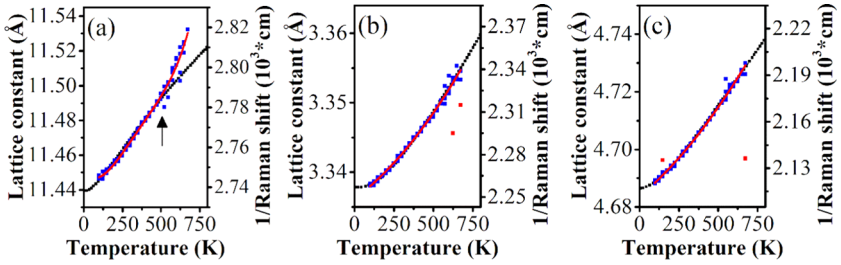

Figure 5. Raman shift temperature dependence for the sample BP4S acetone. Calculated lattice constants of black phosphorus as a function of temperature (black).[47] Reciprocal of the Raman shift (peak position) for each vibrational mode (blue square). Raman shift temperature dependence in the stacking direction (A_g^1 mode) (a). The black arrow indicates a temperature of 500 K (a), zigzag direction (B_{2g} mode) (b), and armchair direction (A_g^2 mode) (c) of the BP unit cell.

phosphorene" modified by oxygen adsorption.[13] The coexistence of the different types of oxides is expected as their energies are degenerate in relation to the full oxidized forms (P_2O_5).[5,18,34] Edmonds et al. detected bridging and dangling oxygens on the surface of air-oxidized bulk black phosphorus.[20] In agreement with theoretical studies, the electronic properties of black phosphorus were altered by oxidation: the work-function had small variations of only 0.1 eV in comparison to pristine bulk black phosphorus, but the electronic band gap had a large modulation (>4.5 eV). From the photoelectron spectroscopy measurements,[20,23] the presence of bridging, dangling, and P_2O_5 was related to peaks centered at 131.54, 132.67, and 134.46 eV, respectively.

Our XPS measurements on acetone-exfoliated black phosphorus (AsEx) coated on a silicon wafer are shown in Figure 4. After 21 days of air oxidation (Figure 4b), a slight broadening of the peak at 133.5 eV was measured (i.e., FWHM: 1.8 and 2.4 eV for the sample at starting time and 21 days later, respectively) in agreement with the previous reports.[29] Edmonds et al. with synchrotron-based photoelectron spectroscopy reported the appearance of two peaks at 131.5 and 132.7 eV related with bridging and dangling oxygen bonding, respectively.[20] In our measurements, we detected a broad peak in the same region (132.4 eV), but diminished with the increasing intensity of the peak corresponding to phosphorus pentoxide (P_2O_5) at 133.5 eV.

The exfoliated flakes were analyzed by TEM (Figure S3) to evaluate the crystal structure after controlled oxygen exposition. From the electron diffractions, no major modifications were detected in the zigzag and armchair directions in agreement with our previous studies.[41] X-ray diffraction (XRD) patterns were collected after cycles of oxygen exposition at 523 K (Figure S4), but no modifications in the stacking direction were detected. The lattice constants calculated for the exfoliated materials are *a:* 3.3 Å, *b:* 4.3 Å, and *c:* 10.8 Å, even after the oxygen exposition, suggesting that the surface oxide is the predominant form and showing the reversibility (Figures S4 and S5) of the process as indicated by DSC results. Altogether, these results confirm the presence of the surface type of oxides.

In the dangling configuration, the oxygen atoms bond to the surface at the zigzag ridge (Figure 1) and the P−O bonds in the dangling position form an angle of 44.5° from the surface.[10,18,24] Herein, the differences in electronegativity between P and O atoms polarize the surface[18] with different implications[9] (i.e., "water bubbles" formation[25]). We suggest that the geometry of surface oxides and their polarization effect explain the blue shift detected in some of the samples under evaluation (Figures S1 and S2). Interestingly, monotonic blue shift for the P═O stretching mode has been proposed for the detection of dangling oxygens;[5] however, it has not been reported in the literature with conventional Raman spectroscopy.

The Raman shift temperature dependence (temperature range: 98.15−673.15 K) was evaluated for a drop-cast sample (i.e., BP4S acetone) mounted on a temperature-controlled probe stage (HFS600E, Linkam). The stage was fed with argon at a rate of 200 mL min^{-1}. The spectra were fitted with Lorentzian functions, and the center of the peaks was tabulated against the corresponding temperature. In Figure 5, reciprocal Raman shift was plotted against temperature (blue squares) and overlaid on the thermal expansion of the lattice constants, as calculated by Villegas et al.[47] (black). For temperatures lower than 500 K (220 °C), A_g^1, B_{2g}, and A_g^2 vibrational modes exhibit good agreement with the lattice constants in the stacking, zigzag, and armchair directions. These results agree with previous reports with a 4 nm thick layer.[48] More interestingly, Figures 5a and 2b−c show an endothermic process starting at approximately 493 K (220 °C) and in situ Raman spectroscopy localized this process in the stacking

DOI: 10.1021/acsomega.8b01989
ACS Omega 2018, 3, 12482−12488

direction (A_g^1 vibrational mode), in agreement with our proposed model for the thermal analysis, but this effect was not visible in thicker layers[48] possibly because the oxidation happens only at the topmost layer[20] and measurements with thicker samples hinder the effect on the Raman spectra. As expected, the dangling to interstitial transition requires an additional expansion in the stacking direction to place oxygen atoms in between two phosphorus atoms in the stacking direction, and this endothermic process can be followed by in situ Raman spectroscopy and DSC.

During the Raman spectra measurements, four spectra were consecutively collected at each temperature to analyze the laser effect. The standard deviation for the peak position during consecutive samples (time between consecutive samples: <30 s) is negligible (standard deviation <0.5 cm^{-1} for temperatures lower than 500 K) in comparison to the thermal effect controlled by the stage. Even though local heating is produced during laser exposure, no laser-induced chemical modifications were detected during the Raman measurement according to the standard deviations (Figure S6 in the Supporting Information).

The thermal expansion coefficients and phonon frequencies at 0 K shown in Table 2 were calculated from the linear fit

Table 2. Linear Fitting Parameters for the Raman Shift Temperature Dependence[a]

vibrational mode	slope, χ (cm^{-1} K^{-1})	intercept, ω_0 (cm^{-1})	R^2
A_g^1	−0.015	366.4	0.98
B_g^2	−0.027	446.5	0.99
A_g^2	−0.028	475.3	0.99

[a]Temperature range: 290−485 K.

parameters of the Raman shift temperature dependence (Figure 5), according to the Grüneisen model in eq 1. These results are in good agreement with previous reports[49,50] for evaluations in the temperature range of 293−433 K.

$$\omega(T) = \omega_0 + \chi T \quad (1)$$

The correlation between the lattice expansion and the Raman shift shown in Figure 5 can be described by the following mathematical model, where $[\omega_0 + \chi T]$ corresponds to the Grüneisen model parameters corresponding to each vibrational mode, and a, b, and c are the lattice constants

$$a = 25.762 - 0.101 \times [\omega_0(B_{2g}) + \chi(B_{2g})T] + 1.129 \times 10^{-4} \times [\omega_0(B_{2g}) + \chi(B_{2g})T]^2$$

$$b = 5.873 - 0.00251 \times [\omega_0(A_g^2) + \chi(A_g^2)T]$$

$$c = 14.459 - 0.00826 \times [\omega_0(A_g^1) + \chi(A_g^1)T]$$

Herein, we propose the previous mathematical model as a baseline to evaluate the modifications of the lattice caused by processes like oxidation or interstitial intercalation/doping in the temperature range of 200−450 K for few-layer systems. The R-square coefficients for the three equations were 0.995, 0.9996, and 0.9995 for the lattice constants a, b, and c, respectively.

Ziletti et al. calculated the band gap dependence on the number of oxygen atoms per unit cell. For surface oxides, the calculated band gap was approximately 2.5 eV for two or four oxygen atoms per unit cell; however, for the planar form (i.e., in the presence of interstitial oxygen), the calculated band gap exhibited a monotonic increase with the number of oxygen atoms per unit cell (Table 3). Therefore, controlling the type of oxide and the number of oxygen atoms in the unit cell enables opportunities for the band gap engineering in black phosphorus.[5]

Table 3. Band Gap Energy Calculated with HSE as a Function of the Number of Oxygen Atoms Per Unit Cell[a]

type of oxide	number of oxygen atoms per unit cell	band gap (eV)
surface	2	2.5
	4	2.3
planar	2	3.4
	4	4.1

[a]Adapted from ref 5.

Experimentally, water bubbles formation at the surface of exfoliated BP has been used as an indicator of oxidation.[24] Here, a quantitative tool for tracking the oxidation of black phosphorus and few-layer BP by backscattering Raman is shown. We have described a proposed model based on the evidence from thermal analysis (TGA, DSC), Raman spectroscopy, in situ TEM, XRD, photoelectron spectroscopy, and theoretical studies as a contribution on the required understanding of black phosphorus oxidation.

3. CONCLUSIONS

Different types of oxides coexist in air-oxidized bulk black phosphorus.[20,23] Theoretical studies provide insightful results: fully oxidized compounds and intermediate states have close binding energy values.[5] Herein, our samples contain several kinds of oxides, and oxygen-poor forms are present even after 28 days of air exposition.[20] Theoretically, the oxygen adsorption is an exothermic process and the dangling position is 0.69 eV[18] more energetically favorable than the bridging and interstitial positions. The first stages of oxidation are characterized by slight or no alteration of the Raman spectra, while the Raman shift temperature dependence reveals a process in the stacking direction occurring at 493 K. This result was congruent with our reported thermogravimetric analysis.

In situ Raman spectroscopy shows a good fitting between the lattice constants and theoretical thermal expansion of the unit cell and validates previous theoretical calculations on black phosphorus oxidation. This work unlocks opportunities for applications of band gap engineering with black phosphorus native oxides. We propose a simple mathematical model to track deformations in the lattice structure by using the Grüneisen and the fitting between Raman and lattice temperature dependence.

From the thermal analysis, we report the decomposition of bulk black phosphorus (sublimation[43]) at approximately 703 K in oxidative media. Additionally, we report an inflection point at approximately 493 K, where the oxygen uptake is exponentially observed and might be considered as an operational restriction limit for the usage of black phosphorus in certain applications. Transitions were visible in DSC measurements at approximately 528 K for heating ramps of 5 K min^{-1}, and we relate them to surface (dangling, bridging) to interstitial oxygen-bonding transformations, as seen by in situ Raman spectroscopy.

DOI: 10.1021/acsomega.8b01989
ACS Omega 2018, 3, 12482−12488

4. METHODS

4.1. Few-Layer Black Phosphorus Preparation. Bulk black phosphorus crystal was purchased from HQ Graphene (Groningen, The Netherlands) and stored in the dark and argon atmosphere. The exfoliation method was ultrasonication in a 120 W, 35 kHz bath. Bulk BP crystals (5 mg) were added to 13 mL of acetone in a glass vial tightly closed with a septum cap. The mixture was bubbled with argon to drive out the dissolved oxygen from the solvent and the free space inside the vial. The temperature during the sonication was kept constant at 298 K, and the sonication time was fixed to 24 h. After the ultrasonication period, the sample was allowed to sediment for 24 h, after which the supernatant was collected and marked as AsEx. This sample was flushed with argon and stored for additional characterization. Another fraction was collected from the sample AsEx and centrifuged at 2000 rpm for 30 min. The supernatant was collected, flushed, and labeled as BP2S. From the sample BP2S, another fraction was collected and centrifuged at 4000 rpm for 30 min. The supernatant was collected, flushed, and labeled as BP4S.

4.2. Few-Layer Black Phosphorus Characterization. Raman characterization was performed at the excitation wavelength of 532 nm and a nominal laser power of 12.5 mW (Senterra, Bruker). The sample was drop-cast on either glass microscope slides or silicon wafers as the substrate. The samples were characterized using a well-defined optical objective (Olympus) to ensure that the scanning area, laser power, and wavelength were the same for all samples. The spectral resolution was set to ca. 3−5 cm^{-1}, and the interferometer resolution was 1.5 cm^{-1}. All of the spectra were collected using three coadditions of 5 s each and taken at random locations on the few-layer BP clusters over time.

Thermogravimetric analysis (TA Instruments, Q500, TGA) was conducted using a platinum sample holder in oxidative atmosphere (synthetic air) at a heating ramp of 5 K min^{-1}. Differential scanning calorimetry (TA Instruments, Q20, DSC) was carried out using an aluminum sample holder (pan + lid) in nitrogen atmosphere at a heating ramp of 5 K min^{-1}. The baseline was taken with empty sample holders (pan + lid) for the DSC measurements.

The absorption spectra in the UV−vis−NIR region were measured in a spectrophotometer (Hitachi, U-2001) with a sweep speed of 100 nm min^{-1}. The scanning window was set between 300 and 1100 nm. The samples were placed in a quartz high-precision cell with a light path of 10 mm (Hellma Analytics).

The hydrodynamic size and zeta potentials of the suspensions were measured by dispersed light scattering (Zetasizer Nano ZS, Malvern) at a wavelength of 633 nm. The refractive index utilized for the few-layer BP was 3.4.[51,52] For acetone, the refractive index and the dynamic viscosity values at room temperature were 1.356 and 0.3111 mPa s, respectively.

ASSOCIATED CONTENT

Supporting Information

The Supporting Information is available free of charge on the ACS Publications website at DOI: 10.1021/acsomega.8b01989.

Additional information on the Raman spectra, TEM, and XRD evaluation (PDF)

AUTHOR INFORMATION

Corresponding Author

*E-mail: kakos@chem.u-szeged.hu.

ORCID

Ákos Kukovecz: 0000-0003-0716-9557

Author Contributions

J.G.P. originated the idea of this work, designed the experiments, carried out some of the experimental work, and wrote the manuscript draft. Additional experimental work was done by B.B. and I.Y.T. Z.K. and A.K. supervised the experimental work and assisted in the interpretation of the results and writing the final manuscript.

Notes

The authors declare no competing financial interest.

ACKNOWLEDGMENTS

The first author (J.G.P.) acknowledges the Administrative Department of Science, Technology, and Innovation of Colombia (*Colciencias*) for the PhD scholarship. Support from the "Széchenyi 2020" program in the framework of GINOP-2.3.2-15-2016-00013 project and the NKFIH K 126065 grant is also acknowledged.

REFERENCES

(1) Keyes, R. W. The electrical properties of black phosphorus. *Phys. Rev.* **1953**, *92*, 580−584.

(2) Doganov, R. A.; O'Farrell, E. C. T.; Koenig, S. P.; Yeo, Y.; Ziletti, A.; Carvalho, A.; et al. Transport properties of pristine few-layer black phosphorus by van der Waals passivation in an inert atmosphere. *Nat. Commun.* **2015**, *6*, No. 6647.

(3) Dhanabalan, S. C.; Ponraj, J. S.; Guo, Z.; Li, S.; Bao, Q.; Zhang, H. Emerging Trends in Phosphorene Fabrication towards Next Generation Devices. *Adv Sci.* **2017**, No. 1600305.

(4) Castellanos-Gomez, A.; Vicarelli, L.; Prada, E.; Island, J. O.; Narasimha-Acharya, K. L.; Blanter, S. I.; et al. Isolation and characterization of few-layer black phosphorus. *2D Mater.* **2014**, *1*, No. 025001.

(5) Ziletti, A.; Carvalho, A.; Trevisanutto, P. E.; Campbell, D. K.; Coker, D. F.; Castro Neto, A. H. Phosphorene oxides: Bandgap engineering of phosphorene by oxidation. *Phys. Rev. B* **2015**, *91*, No. 085407.

(6) Kaur, H.; Yadav, S.; Srivastava, A. K.; Singh, N.; Schneider, J. J.; Sinha, O. P.; et al. Large Area Fabrication of Semiconducting Phosphorene by Langmuir-Blodgett Assembly. *Sci Rep.* **2016**, *6*, No. 34095.

(7) Lu, J.; Yang, J.; Carvalho, A.; Liu, H.; Lu, Y.; Sow, C. H. Light-Matter Interactions in Phosphorene. *Acc. Chem. Res.* **2016**, *49*, 1806−1815.

(8) Ling, X.; Wang, H.; Huang, S.; Xia, F.; Dresselhaus, M. S. The renaissance of black phosphorus. *Proceedings of the National Academy of Sciences* **2015**, *112*, No. 201416581.

(9) Hu, W.; Lin, L.; Zhang, R.; Yang, C.; Yang, J. Highly Efficient Photocatalytic Water Splitting over Edge-Modified Phosphorene Nanoribbons. *J. Am. Chem. Soc.* **2017**, *139*, 15429−15436.

(10) Wang, C.-X.; Zhang, C.; Jiang, J.-W.; Rabczuk, T. The Effects of Vacancy and Oxidation on Black Phosphorus Nanoresonators. *Nanotechnology.* **2017**, *28*, No. 135202.

(11) Sofer, Z.; Bouša, D.; Luxa, J.; Mazanek, V.; Pumera, M. Few-layer black phosphorus nanoparticles. *Chem. Commun.* **2016**, *52*, 1563−1566.

(12) Xiao, K. J.; Carvalho, A.; Castro Neto, A. H. Defects and oxidation resilience in InSe. *Phys. Rev. B* **2017**, *96*, No. 054112.

(13) Malyi, O. I.; Sopiha, K. V.; Draxl, C.; Persson, C. Stability and electronic properties of phosphorene oxides: from 0-dimensional to amorphous 2-dimensional structures. *Nanoscale* **2017**, *9*, 2428−2435.

DOI: 10.1021/acsomega.8b01989
ACS Omega 2018, 3, 12482−12488

(14) Guo, Y.; Zhou, S.; Bai, Y.; Zhao, J. Oxidation Resistance of Monolayer Group-IV Monochalcogenides. *ACS Appl. Mater. Interfaces* **2017**, *9*, 12013−12020.
(15) Wang, G.; Pandey, R.; Karna, S. P. Physics and chemistry of oxidation of two-dimensional nanomaterials by molecular oxygen. *Wiley Interdiscip. Rev.: Comput. Mol. Sci.* **2017**, *7*, No. e1280.
(16) Abellán, G.; Wild, S.; Lloret, V.; Scheuschner, N.; Gillen, R.; Mundloch, U.; et al. Fundamental Insights into the Degradation and Stabilization of Thin Layer Black Phosphorus. *J. Am. Chem. Soc.* **2017**, *139*, 10432−10440.
(17) Ribeiro, H. B.; Pimenta, M. A.; de Matos, C. J. S. Raman spectroscopy in black phosphorus. *J. Raman Spectrosc.* **2017**, 76−90.
(18) Ziletti, A.; Carvalho, A.; Campbell, D. K.; Coker, D. F.; Castro Neto, A. H. Oxygen defects in phosphorene. *Phys. Rev. Lett.* **2015**, *114*, No. 046801.
(19) Han, C.; Hu, Z.; Carvalho, A.; Guo, N.; Zhang, J.; Hu, F.; et al. Oxygen induced strong mobility modulation in few-layer black phosphorus. *2D Mater.* **2017**, *4*, No. 021007.
(20) Edmonds, M. T.; Tadich, A.; Carvalho, A.; Ziletti, A.; O'Donnell, K. M.; Koenig, S. P.; et al. Creating a stable oxide at the surface of black phosphorus. *ACS Appl. Mater. Interfaces* **2015**, *7*, 14557−14562.
(21) Nahas, S.; Ghosh, B.; Bhowmick, S.; Agarwal, A. First-principles cluster expansion study of functionalization of black phosphorene via fluorination and oxidation. *Phys. Rev. B* **2015**, *93*, No. 165413.
(22) Carvalho, A.; Castro Neto, A. H. Phosphorene: Overcoming the oxidation barrier. *ACS Cent. Sci.* **2015**, *1*, 289−291.
(23) Kuntz, K. L.; Wells, R. A.; Hu, J.; Yang, T.; Dong, B.; Guo, H.; et al. Control of Surface and Edge Oxidation on Phosphorene. *ACS Appl. Mater. Interfaces* **2017**, *9*, 9126−9135.
(24) Wang, G.; Slough, W. J.; Pandey, R.; Karna, S. P. Degradation of phosphorene in air: understanding at atomic level. *2D Mater.* **2016**, *3*, No. 025011.
(25) Utt, K. L.; Rivero, P.; Mehboudi, M.; Harriss, E. O.; Borunda, M. F.; San Juan, A. A. P.; et al. Intrinsic defects, fluctuations of the local shape, and the photo-oxidation of black phosphorus. *ACS Cent. Sci.* **2015**, *1*, 320−327.
(26) Kistanov, A. A.; Cai, Y.; Zhou, K.; Dmitriev, S. V.; Zhang, Y.-W. The role of H2O and O2 molecules and phosphorus vacancies in the structure instability of phosphorene. *2D Mater.* **2017**, *4*, No. 015010.
(27) Favron, A.; Gaufres, E.; Fossard, F.; Phaneuf-L'Heureux, A.-L.; Tang, N. Y.-W.; Levesque, P. L.; et al. Photooxidation and quantum confinement effects in exfoliated black phosphorus. *Nat. Mater.* **2015**, *14*, 826−832.
(28) Stachel, D.; Svoboda, I.; Fuess, H. Phosphorus Pentoxide at 233 K. *Acta Crystallogr., Sect. C: Cryst. Struct. Commun.* **1995**, *51*, 1049−1050.
(29) Woomer, A. H.; Farnsworth, T. W.; Hu, J.; Wells, R. A.; Donley, C. L.; Warren, S. C. Phosphorene: Synthesis, Scale-Up, and Quantitative Optical Spectroscopy. *ACS Nano.* **2015**, *9*, 8869−8884.
(30) Hu, Z.; Li, Q.; Lei, B.; Zhou, Q.; Xiang, D.; Lyu, Z.; et al. Water-Catalyzed Oxidation of Few-Layer Black Phosphorous in a Dark Environment. *Angew. Chem., Int. Ed.* **2017**, *56*, 9131−9135.
(31) Lü, T.-Y.; Feng, H.; Zhang, Y.; Lu, Y.; Zheng, J.-C. Regulate the polarity of phosphorene's mechanical properties by oxidation. *Comput. Mater. Sci.* **2017**, *139*, 341−346.
(32) Boukhvalov, D. W.; Rudenko, A. N.; Prishchenko, D. A.; Mazurenko, V. G.; Katsnelson, M. I. Chemical modifications and stability of phosphorene with impurities: a first principles study. *Phys. Chem. Chem. Phys.* **2015**, *17*, 15209−15217.
(33) Marcia, M.; Hirsch, A.; Hauke, F. Perylene-based non-covalent functionalization of 2D materials. *FlatChem* **2017**, *1*, 89−103.
(34) Drissi, L. B.; Sadki, S.; Sadki, K. Half-oxidized phosphorene: band gap and elastic properties modulation. *J. Phys. Condens. Matter* **2016**, *28*, No. 145501.
(35) Suryawanshi, S. R.; More, M. A.; Late, D. J. Laser exfoliation of 2D black phosphorus nanosheets and their application as a field emitter. *RSC Adv.* **2016**, *6*, 112103−112108.
(36) Lu, W.; Nan, H.; Hong, J.; Chen, Y.; Zhu, C.; Liang, Z.; et al. Plasma-assisted fabrication of monolayer phosphorene and its Raman characterization. *Nano Res.* **2014**, *7*, 853−859.
(37) Abellán, G.; Neiss, C.; Lloret, V.; Wild, S.; Chacón-Torres, J. C.; Werbach, K.; et al. Exploring the Formation of Black Phosphorus Intercalation Compounds with Alkali Metals. *Angew. Chem., Int. Ed.* **2017**, *56*, 15267−15273.
(38) Ling, Z.-P.; Zhu, J.-T.; Liu, X.; Ang, K.-W. Interface Engineering for the Enhancement of Carrier Transport in Black Phosphorus Transistor with Ultra-Thin High-k Gate Dielectric. *Sci. Rep.* **2016**, *6*, No. 26609.
(39) Galceran, R.; Gaufres, E.; Loiseau, A.; Piquemal-Banci, M.; Godel, F.; Vecchiola, A.; et al. Stabilizing ultra-thin black phosphorus with in-situ-grown 1 nm-Al2O3 barrier. *Appl. Phys. Lett.* **2017**, *111*, No. 243101.
(40) Ryder, C. R.; Wood, J. D.; Wells, S. A.; Yang, Y.; Jariwala, D.; Marks, T. J.; et al. Covalent functionalization and passivation of exfoliated black phosphorus via aryl diazonium chemistry. *Nat. Chem.* **2016**, *8*, 597−602.
(41) Gómez-Pérez, J.; Kónya, Z.; Kukovecz, Á. Acetone improves the topographical homogeneity of liquid phase exfoliated few-layer black phosphorus flakes. *Nanotechnology* **2018**, *29*, No. 365303.
(42) Wang, X.; Jones, A. M.; Seyler, K. L.; Tran, V.; Jia, Y.; Zhao, H.; et al. Highly anisotropic and robust excitons in monolayer black phosphorus. *Nat. Nanotechnol.* **2015**, *10*, 517−521.
(43) Liu, X.; Wood, J. D.; Chen, K. S.; Cho, E.; Hersam, M. C. In situ thermal decomposition of exfoliated two-dimensional black phosphorus. *J. Phys. Chem. Lett.* **2015**, *6*, 773−778.
(44) Brazhkin, V. V.; Zerr, A. J. Relative stability of red and black phosphorus at P < 1 GPa. *J. Mater. Sci.* **1992**, *27*, 2677−2681.
(45) Alsaffar, F.; Alodan, S.; Alrasheed, A.; Alhussain, A.; Alrubaiq, N.; Abbas, A.; et al. Raman Sensitive Degradation and Etching Dynamics of Exfoliated Black Phosphorus. *Sci. Rep.* **2017**, *7*, No. 44540.
(46) Iacopi, F.; Boeckl, J. J.; Jagadish, C. *2D Materials*, 1st ed.; Jagadish, C., Weber, E. R., Eds.; Elsevier Inc: Cambridge, 2016.
(47) Villegas, C. E.; Rocha, A. R.; Marini, A. Anomalous Temperature Dependence of the Band Gap in Black Phosphorus. *Nano Lett.* **2016**, *16*, 5095−5101.
(48) Late, D. J. Temperature Dependent Phonon Shifts in Few-Layer Black Phosphorus. *ACS Appl. Mater. Interfaces* **2015**, *7*, 5857−5862.
(49) Zhang, S.; Yang, J.; Xu, R.; Wang, F.; Li, W.; Ghufran, M.; et al. Extraordinary photoluminescence and strong temperature/angle-dependent raman responses in few-layer phosphorene. *ACS Nano* **2014**, *8*, 9590−9596.
(50) Luo, Z.; Maassen, J.; Deng, Y.; Du, Y.; Garrelts, R. P.; Lundstrom, M. S.; et al. Anisotropic in-plane thermal conductivity observed in few-layer black phosphorus. *Nat. Commun.* **2015**, *6*, No. 8572.
(51) Yang, J.; Xu, R.; Pei, J.; Myint, Y. W.; Wang, F.; Wang, Z. et al. Unambiguous identification of monolayer phosphorene by phase-shifting interferometry. **2014**, arXiv preprint arXiv:1412.6701.
(52) Nagahama, T.; Kobayashi, M.; Akahama, Y.; Endo, S.; Narita, S. Optical Determination of Dielectric Constant in Black Phosphorus. *J. Phys. Soc. Jpn.* **1985**, *54*, 2096−2099.

DOI: 10.1021/acsomega.8b01989
ACS Omega 2018, 3, 12482−12488